International Journal of Nanomedicine

Dovepress
Taylor & Francis Group

Open Access Full Text Article

ORIGINAL RESEARCH

ZnO Nanocrystals Inhibit *Escherichia coli* Biofilms by Suppressing *glgA*- and *gltB*-Dependent EPS Biosynthesis

Xinyuan Tian[1], Chaoyu Zhou[1], Qianyu Bai[1], Yinzhu Chen[1], Runqiu Cai[1], Jiaxin Lai[1], Linyi Ye[1], Wanru Feng[1], Yeru Wang[2], Qingyi Song[3], Tianlong Liu[1]

[1]State Key Laboratory of Veterinary Public Health and Safety, China Agricultural University, Beijing, People's Republic of China; [2]Risk Assessment Department, China National Center for Food Safety Risk Assessment, Beijing, People's Republic of China; [3]Anyang CAU Biotechnology Co., Ltd, Anyang, Henan, People's Republic of China

Correspondence: Tianlong Liu, State Key Laboratory of Veterinary Public Health and Safety, China Agricultural University, Beijing, 100193, People's Republic of China, Email liutianlong@cau.edu.cn; Yeru Wang, Risk Assessment Department, China National Center for Food Safety Risk Assessment, Building 2, No. 37, Guangqu Road, Chaoyang District, Beijing, 100022, People's Republic of China, Email wangyeru@cfsa.net.cn

Introduction: Bacterial biofilms are a major cause of persistent and device-related infections due to their antibiotic resistance and ability to shelter bacteria. Zinc oxide nanocrystals (ZnO NCs), with their multiple antimicrobial mechanisms, have emerged as efficient antibacterial agents.

Methods: In this study, we synthesized rod-shaped ZnO NCs and evaluated their anti-biofilm efficacy against *Escherichia coli*. Anti-biofilm activity was assessed at sub-minimum inhibitory concentration (MIC) and MIC levels. Transcriptomic analysis and qPCR were employed to examine gene expression changes in *E. coli*, with further mechanistic validation targeting specific metabolic pathways.

Results: At sub-MIC levels, ZnO NCs potently inhibited biofilm formation and eradicated pre-formed *E. coli* biofilms. These treatments also markedly suppressed the synthesis of key extracellular polymeric substances (EPS) components, while MIC-level treatments effectively degraded existing EPS in mature biofilms. Concurrently, ZnO NCs reduced overall EPS density, loosened biofilm architecture, and increased its structural heterogeneity. Furthermore, bacterial motility (swimming, twitching, and swarming) was strongly impaired across sub-MIC to MIC concentrations. Transcriptomic analysis revealed that ZnO NCs downregulated genes associated with biofilm formation, motility, and amino acid biosynthesis. qPCR indicated that the downregulation of *glgA* and *gltB* impaired the synthesis of key EPS components.

Conclusion: Mechanistically, we validate that in *E. coli*, ZnO NCs suppress *glgA* to disrupt glycogen-derived carbon precursors for polysaccharide synthesis, and downregulate *gltB* to impair glutamate synthase activity, thereby limiting nitrogen assimilation and amino acid supply for proteinaceous EPS components. These findings elucidate a previously undefined mechanism wherein ZnO NCs dismantle *E. coli* biofilms by simultaneously targeting two pivotal metabolic nodes (*glgA* and *gltB*) that fuel EPS production. This work provides not only a deeper mechanistic insight into anti-biofilm action against *E. coli* but also supports the potential of ZnO NCs as multi-targeted anti-biofilm agents.

Keywords: nanotoxicology, antibiofilm, extracellular polymeric substances, motility, bacterial stress response

Introduction

Bacterial biofilm is a highly organized community formed by microorganisms to adapt to complex environment. The essence of bacterial biofilm is a three-dimensional structure formed by bacteria to wrap themselves and adhere to biological or non-biological surfaces by secreting Extracellular Polymeric Substances (EPS).[1] The core component of biofilm is EPS, accounting for 50% to 90% of its dry weight, mainly including polysaccharides, proteins, extracellular DNA (eDNA) and lipids.[2] These substances form physical barriers through hydrogen bonding, hydrophobic interaction and cation bridging, which not only provide mechanical protection for bacteria, but also trap water and nutrients and maintain a stable internal microenvironment.[3–5] The function of biofilm is dual: on the one hand, it enhances the

https://doi.org/10.2147/IJN.S583878
Received: 23 November 2025
Accepted: 27 February 2026
Published: 8 June 2026

Graphical Abstract

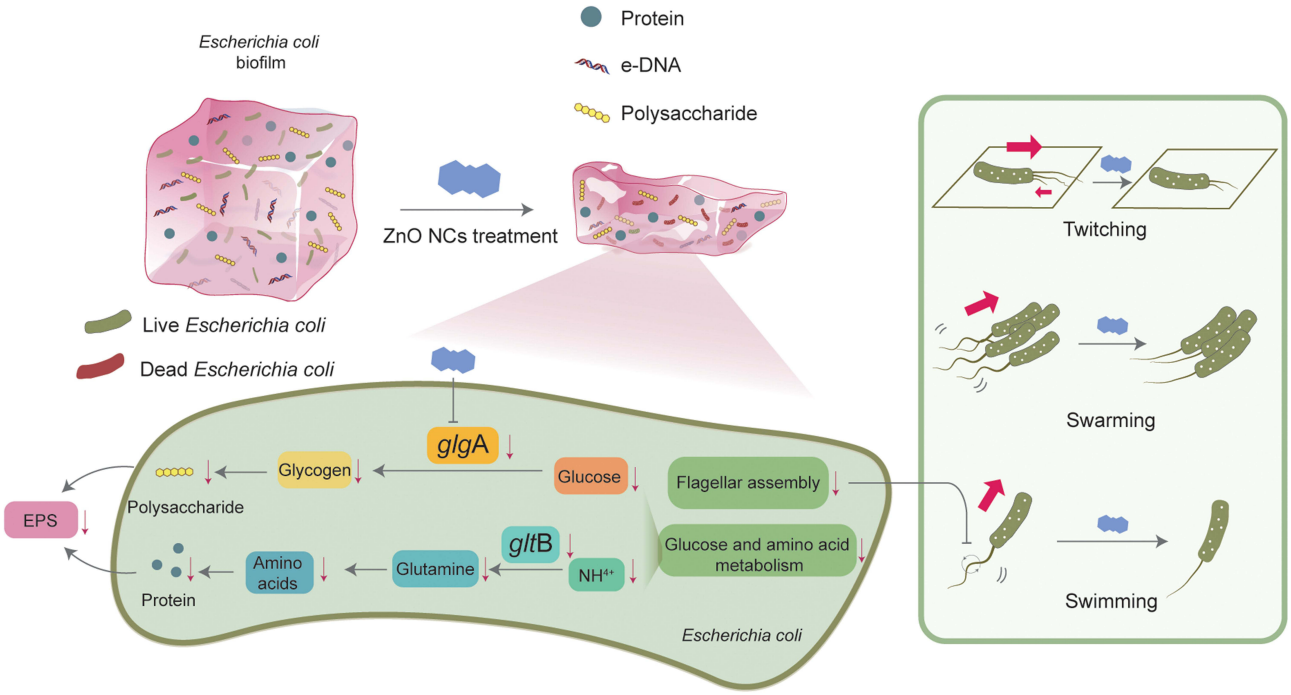

colonization ability of bacteria in the host or environment, promotes interspecific cooperation and horizontal gene transfer; On the other hand, the harm it causes is extremely serious, such as chronic infections, medical device-associated infections, and industrial pipe clogs and biocorrosion.[6,7] Therefore, there is a pressing need to develop treatment strategies specifically targeting biofilms to address their remarkable drug resistance.

Extracellular polymeric substances (EPS) constitute the key structural and functional basis for biofilm infectivity and drug resistance. Polysaccharides such as alginate, galactose, mannose, and glucuronic acid form a cross-linked scaffold that provides mechanical stability and limits antibiotic diffusion.[8] Proteins including adhesins like LapA in *Pseudomonas fluorescens* mediate bacterial attachment to surfaces and initiate infection.[9] Amyloid proteins (eg, curli fibers in *Escherichia coli* (*E. coli*)) promote cell aggregation and immune evasion, reinforcing infection persistence.[10,11] The biofilm matrix is reinforced by eDNA through cation chelation and facilitates horizontal gene transfer of antibiotic resistance genes.[12,13] Bacterial motility is essential for surface exploration, initial attachment, and biofilm expansion,[14] though it is suppressed upon maturation to promote entrapment within EPS.[15,16] The EPS matrix confers drug resistance by limiting antibiotic penetration, adsorbing antimicrobial agents, and sheltering persister cells from immune clearance.[17,18] Importantly, motility affects EPS secretion and organization, while EPS architecture reciprocally influences motility and attachment dynamics.[19,20] This bidirectional physico-biochemical interplay, orchestrated by the precise genetic regulation of processes such as quorum sensing, EPS synthesis, and flagellar assembly, collectively constitutes a "biofilm integrity system". This system integrates three core pillars: (1) the structural scaffold (EPS), (2) the adaptive behavior (motility), and (3) the underlying genetic regulatory network. It is this integrated system that ensures biofilm cohesion, stability, resistance, and ultimately, its recalcitrance to treatment. Among the genes associated with biofilms, *glgA* and *gltB* are, respectively, associated with different components of EPS in *E. coli* biofilms. The *glgA* gene encodes glycogen synthase, a key enzyme in bacterial glycogen synthesis. Glycogen serves as an intracellular polysaccharide reserve, and its metabolism is closely linked to the synthesis of extracellular polysaccharides (EPS), acting as a precursor pool or carbon source for other EPS components such as capsular polysaccharides and mucoid polysaccharides.[21] The *gltB* gene encodes the large subunit of glutamate synthase (GOGAT),

which together with glutamine synthetase (GS, encoded by) forms the GS-GOGAT pathway, the primary route for nitrogen assimilation in E. coli. This pathway converts glutamine and α-ketoglutarate into two molecules of glutamate, thereby regulating intracellular amino nitrogen balance. It has been shown that *gltB* gene is involved in the formation of bacterial biofilms.[22–24] Together, *glgA* supports biofilm matrix formation by providing glycogen-derived carbon precursors for extracellular polysaccharides, while *gltB* contributes through its role in glutamate synthase-mediated nitrogen metabolism essential for biofilm development. Consequently, therapeutic approaches that target the bacterial biofilm Integrity System represent a critical strategic approach for combating biofilms and treating biofilm-associated infections.

Antimicrobial nanomaterials, particularly metal-based variants, hold significant potential as alternatives or adjuvants to antibiotics for treating bacterial infections. Recent advances in antibacterial materials, such as cationic hydrogels with inherent antimicrobial properties and polydopamine nanoparticle-dotted hydrogels, have demonstrated effective antibacterial and wound-healing capabilities in infected wound models, highlighting the importance of multifunctional strategies for combating biofilm-associated infections.[25,26] Zinc oxide nanocrystals (ZnO NCs) stand out among these materials as a prominent antibacterial agent due to their favorable safety profile, potent antibacterial efficacy, ideal integration into wound dressings, and synergistic interactions with antibiotics.[27] Beyond targeting planktonic bacteria, ZnO NCs also exhibit robust antibiofilm capabilities. Both pristine ZnO NCs and ZnO-based nanocomposites demonstrate broad-spectrum activity against biofilms formed by diverse Gram-positive and Gram-negative pathogens, including *Staphylococcus aureus*, Pseudomonas aeruginosa, *Escherichia coli*, Campylobacter jejuni, Porphyromonas gingivalis, and Serratia marcescens.[28–31] The established antibacterial mechanisms of ZnO NCs encompass: (1) zinc ion dissolution, wherein released Zn^{2+} disrupts bacterial enzyme systems and amino acid metabolism, thereby impairing physiological functions; (2) reactive oxygen species (ROS) generation, as photo-induced electron-hole pairs catalyze oxidative reactions to produce hydroxyl radicals (·OH), hydrogen peroxide (H_2O_2), and other ROS that inflict oxidative damage on DNA, proteins, and lipids; (3) physical disruption via electrostatic adsorption of positively charged ZnO NCs onto negatively charged bacterial membranes, coupled with direct membrane penetration by their sharp-edged structures.[32] In addition, ZnO NCs can induce genetic expression inhibition, evidenced by suppression of core quorum sensing (QS) regulators including *gtfB* and *gtfC* in *Streptococcus mutans*, *lasI, lasR, rhlI*, and *rhlR* in *Pseudomonas aeruginosa*, the *agr* system in methicillin-resistant *Staphylococcus aureus* (MRSA), and the MRSA adhesion-associated *icaA* gene.[33–35] However, most prior studies on ZnO NCs' anti-biofilm effects have focused on phenotypic observations. A systems-level understanding of how ZnO NCs perturb the transcriptional landscape of *E. coli*, specifically to disrupt the biofilm integrity system by targeting its EPS and motility components, is still lacking. This knowledge gap limits the rational development of enhanced nano-antibiofilm strategies.

Thus, we hypothesize that ZnO NCs exert their anti-biofilm activity by disrupting the biofilm integrity system of *E. coli*. To test this, rod-shaped ZnO NCs were first synthesized via a methanol-assisted solvothermal method. We then systematically evaluated their efficacy in inhibiting biofilm formation and eradicating mature biofilms at sub-inhibitory concentrations, and further assessed their impacts on bacterial motility, as well as the composition and architecture of extracellular polymeric substances (EPS). To uncover the underlying molecular mechanism, transcriptomic analysis was employed to identify key pathways perturbed by ZnO NCs. Finally, the roles of critical genes (*glgA* and *gltB*) within these pathways were validated by qPCR. This integrated approach, from phenotypic characterization to transcriptomic profiling and genetic validation, aims to provide a mechanistic explanation for how ZnO NCs compromise the biofilm integrity system.

Materials and Methods

General Experimental Design and Replication

Unless otherwise specified, all quantitative experiments were independently repeated at least three times (biological replicates). Results are presented as the mean ± standard deviation (SD) from at least three independent experiments. The sample size (n) reported in the figure legends corresponds to the number of independent experiments (biological replicates).

Preparation of ZnO NCs

The synthesis of ZnO nanocrystals (NCs) was conducted following the protocol described by Xiangyang Bai et al[36] Briefly, zinc acetate dihydrate and dimethyl sulfone were dissolved in methanol under continuous stirring at 65°C. After 1 hour of reaction, a potassium hydroxide methanol solution was slowly added using a peristaltic pump, and the reaction was continued for an additional 1.5 hours. The resulting product was centrifuged at 10,000 rpm and 4°C for 5 minutes, washed three times with methanol, and finally dried to obtain ZnO NCs.

Characterization of ZnO NCs

SEM

The ZnO NCs methanol solution was diluted to approximately 0.1 mg/mL, dropped onto a tin foil-covered SEM stage, dried at 37°C overnight, and sputter-coated with gold before morphological analysis using scanning electron microscopy.

TEM

A diluted ZnO NCs methanol solution was dropped onto a copper grid, air-dried, and observed under transmission electron microscopy. The longitudinal and transverse diameters of ZnO NCs were measured using ImageJ software, with averages calculated from 10 randomly selected particles.

XRD

Freeze-dried ZnO NCs powder was placed on a sample holder and analyzed in a sealed tube.

Hydrodynamic Size and Zeta Potential

The hydrodynamic diameter and zeta potential of ZnO NCs were measured using a nanoparticle analyzer. The NCs were diluted and dispersed in deionized water (pH 7) and LB broth (pH 7), equilibrated for 2 minutes, and analyzed.

Preparation of ZnO NCs for Biological Assays

Prior to antibacterial or anti-biofilm experiments, ZnO NCs methanol solutions were centrifuged at 10,000 rpm and 4°C for 5 minutes, resuspended in sterile deionized water via ultrasonication, and adjusted to desired concentrations.

Bacterial Cultivation

Single colonies of *Staphylococcus aureus* and *Escherichia coli* from LB agar plates were inoculated into LB broth and incubated at 37°C with shaking until reaching the logarithmic growth phase. Bacterial turbidity was adjusted to 0.5 McFarland standard (approximately 1.0×10^8 CFU/mL) using a turbidimeter.

Determination of MIC and MBC for ZnO NCs

The experiment was performed in 96-well plates using *S. aureus* and *E. coli* suspensions diluted to 1.0×106 CFU/mL. Six ZnO NCs concentration groups (500, 250, 125, 62.5, 31.25, and 15.625 μg/mL), a positive control (penicillin), and a negative control were tested in triplicate. After adding bacterial suspensions and ZnO NCs solutions to achieve a final volume of 200 μL per well, the plate was incubated at 37°C for 18–20 hours. For MIC determination, 0.003% resazurin solution was added, followed by 4 hours of incubation. Antibacterial effects were evaluated based on color changes. For MBC determination, 100 μL of each well was spread on LB agar plates and incubated at 37°C for 24 hours to assess bacterial growth.

E. coli Biofilm Growth Curve Analysis

E. coli was adjusted to 1.0×10^6 CFU/mL and added to 24-well plates (1 mL/well). After incubation at 37°C for 12–72 hours, biofilms were washed with PBS, stained with 0.1% crystal violet (20 minutes), fixed with methanol, dissolved in 33% acetic acid, and quantified at 562 nm using a microplate reader (iMark, Bio-Rad, USA). Triplicates were performed for each time point.

ZnO NCs Inhibit E. coli Biofilm Formation

E. coli suspensions (1.0×10^6 CFU/mL) were mixed with ZnO NCs-LB broth at final concentrations of 0, 15.625, 31.25, 62.5, and 125 μg/mL. After 48 hours of incubation at 37°C, biofilms were washed with PBS and analyzed.

ZnO NCs Eradicate Stablished E. coli Biofilms

Established biofilms (48-hour incubation) were treated with ZnO NCs-LB broth (0–125 μg/mL) for 24 hours. Biofilms were washed with PBS and processed for further analysis.

Viable Bacterial Count in ZnO NCs-Treated Biofilms

Biofilms were ultrasonically dispersed in 1 mL PBS, serially diluted, spread on LB agar plates, and incubated at 37°C for 24 hours to determine CFU counts.

Crystal Violet Staining of E. coli Biofilms

Biofilms were stained with 0.1% crystal violet for 20 minutes, washed, air-dried, photographed, dissolved in 33% acetic acid, and measured at 562 nm. Triplicates were performed. In order to eliminate the influence of residual methanol from ZnO NCs during synthesis and separation on the bacterial biofilm, control experiments were conducted using the residual methanol concentrations corresponding to each concentration gradient of ZnO NCs. The residual methanol concentration is calculated by the difference between the precipitate obtained after centrifugation of the methanol solution of ZnO NCs and the powder after drying.

Laser Confocal Observation of E. coli Biofilms

Biofilms grown on glass-bottom 24-well plates were fixed at room temperature with 4% formaldehyde solution for 15 minutes, then stained with SYTO 9 (Invitrogen), CY3 SE, and Calcofluor White Stain (30 minutes, 4°C in the dark), washed, and imaged under a confocal microscope (A1HD25, Nikon, Japan. Excitation wavelengths: 488, 561, and 405 nm).

Extraction and Content Determination of EPS Components in Biofilms

The biofilms were washed three times with PBS, and 1 mL of deionized water was added followed by ultrasonication for 10 minutes to fully disperse the biofilms. The samples were centrifuged at 14,000 rpm and 4 °C for 15 minutes, and the supernatant was collected and filtered through a 0.22 μm filter to remove bacterial cells.

The protein content was determined using a BCA protein quantification kit (Solarbio, China). According to the manufacturer's instructions, bovine serum albumin (BSA) was used as the standard. A 20 μL aliquot of the biofilm dispersion containing soluble EPS was mixed with 200 μL of BCA working reagent and incubated at 37 °C for 30 minutes. The absorbance was measured at 562 nm.

The polysaccharide content was measured according to the method described by Wang et al[37] 1 mL of the supernatant was mixed with 3 mL of ethanol. The mixture was placed at 4 °C overnight. The precipitated polysaccharides were dissolved in 1 mL of distilled water, followed by the addition of 1 mL of 5% phenol. After mixing, 6 mL of concentrated sulfuric acid was added along the tube wall and allowed to react for 30 minutes. Using a 1% glucose solution as the standard, 150 μL of the solution was transferred to a 96-well plate, and the absorbance was measured at 420 nm using a multifunctional microplate reader.

The eDNA concentration was determined using an ultra-micro spectrophotometer (NanoOne-S, Yooning, China). All reported eDNA data are derived from samples meeting this purity standard (A260/A280 ratio >1.8).

Determination of Bacterial Motility

The method for determining bacterial motility can be referred to in the article by Saeki et al[38] Swimming agar plates (1% tryptone, 0.5% NaCl, 0.3% agar, 0–125 μg/mL ZnO NCs) were centrally inoculated with *E. coli* and incubated at 37°C for 24 hours. Swarming agar plates (1% glucose, 0.5% peptone, 0.2% yeast extract, 0.5% agar, 0–125 μg/mL ZnO NCs) were inoculated with 10 μL *E. coli* (1.0×10^8 CFU/mL) and incubated at 37°C for 24 hours. Twitching agar plates (1%

tryptone, 0.5% yeast extract, 1% NaCl, 1% agar, 0–125 μg/mL ZnO NCs) were inoculated at the agar bottom with *E. coli* and incubated at 37°C for 24 hours.

Transcriptomic Study of ZnO NCs Anti-E. coli Biofilm

The *E. coli* suspension was diluted with LB broth to a final concentration of 1.0×10^6 CFU/mL, and 1 mL of the bacterial suspension was added to each well of a 6-well plate. After incubation at 37 °C for 48 hours, the bacterial suspension in each well was gently aspirated and replaced with either LB broth or a ZnO NCs–LB broth mixture to achieve final ZnO NCs concentrations of 0 μg/mL and 31.25 μg/mL, followed by further incubation for 4 hours. The biofilms were then gently washed three times with PBS buffer. Methods for RNA extraction, quality assessment, and subsequent transcriptomic analysis are described in detail in Supplementary Material 1. Strand-specific libraries were constructed from both ZnO NPs-treated and control groups and sequenced on an Illumina platform for paired-end reads. Raw data were quality-controlled using fastp to remove adapters and low-quality reads. After filtering, each sample yielded approximately 22.5 million high-quality paired-end sequences (Clean Reads) on average, with an average Q30 score >95%. Subsequently, Clean Reads were aligned to the *Escherichia coli* reference genome (Assembly: NZ_CP024138.1) using HISAT2. The average mapping rate across all samples exceeded 97%, indicating high data quality suitable for downstream analysis. Detailed data can be found in Table S1.

Real-Time Fluorescence Quantitative PCR Detection

E. coli biofilms were cultured and treated in the same way as described in *Proteomics Study of ZnO NCs anti-E. coli Biofilm*. RNA extraction was performed using the total RNA Extraction Kit for Cultured cells/Bacteria (RNAprep Pure, Tiangen, China). cDNA was synthesized using Evo M-MLV RT Kit with gDNA Clean for qPCR II (Accurate Biotechnology, Hunan, China), and then subjected to qPCR using SYBR Green Premix Pro Taq HS qPCR Kit II (Accurate Biotechnology, Hunan, China) in a Thermo Fisher 7500 Real-Time PCR System (ABI7500, Applied Biosystems, USA). To normalize mRNA abundance, the expression of the *rpo*D gene was used as an internal control. The primer sequences are shown in Table S2.

Statistical Analyses

Data are presented as the mean ± standard deviation (SD) from at least three independent biological replicates. The sample size (n) stated in the figure legends refers to the number of independent experiments. Prior to parametric statistical analysis, the assumptions of normality and homogeneity of variances were assessed using the Shapiro–Wilk test and Brown-Forsythe test, respectively. For comparisons among more than two groups, one-way analysis of variance (ANOVA) was performed. When the overall ANOVA result was significant ($p < 0.05$), Dunnett's post-hoc test was applied for multiple comparisons against a single control group, as it optimally controls the Type I error rate in this design. All analyses were conducted using GraphPad Prism 10.1. One-way ANOVA was applied to assess intergroup differences, with significance levels set at $p > 0.05$ (ns), $p < 0.05$ (*), $p < 0.01$ (**) and $p < 0.001$ (***).

Results and Discussion

The Synthesis and Characterization of ZnO NCs

In this study, ZnO NCs were synthesized using a methanol-based solvothermal method. SEM images revealed that the ZnO NCs exhibited cylindrical or short rod-shaped nanostructures (Figure 1A). TEM analysis further confirmed their rod-like morphology with good dispersion, showing an average longitudinal diameter of approximately 14 nm and a transverse diameter of 4 nm (Figure 1B). X-ray diffraction (XRD) patterns demonstrated that the synthesized ZnO NCs displayed characteristic peaks consistent with the standard ZnO NCs reference card, confirming their crystalline identity (Figure 1C). Dynamic light scattering (DLS) measurements indicated a hydrodynamic diameter of 122.4 ± 13.9 nm for the ZnO NCs, with a positively charged surface exhibiting a zeta potential of 32.4 ± 3.2 mV (Figure 1D and E). To assess the dispersion state and colloidal stability of ZnO NCs under the actual experimental conditions, their hydrodynamic diameter and zeta potential were also measured in the biological assay medium (LB broth). As summarized in Table S3,

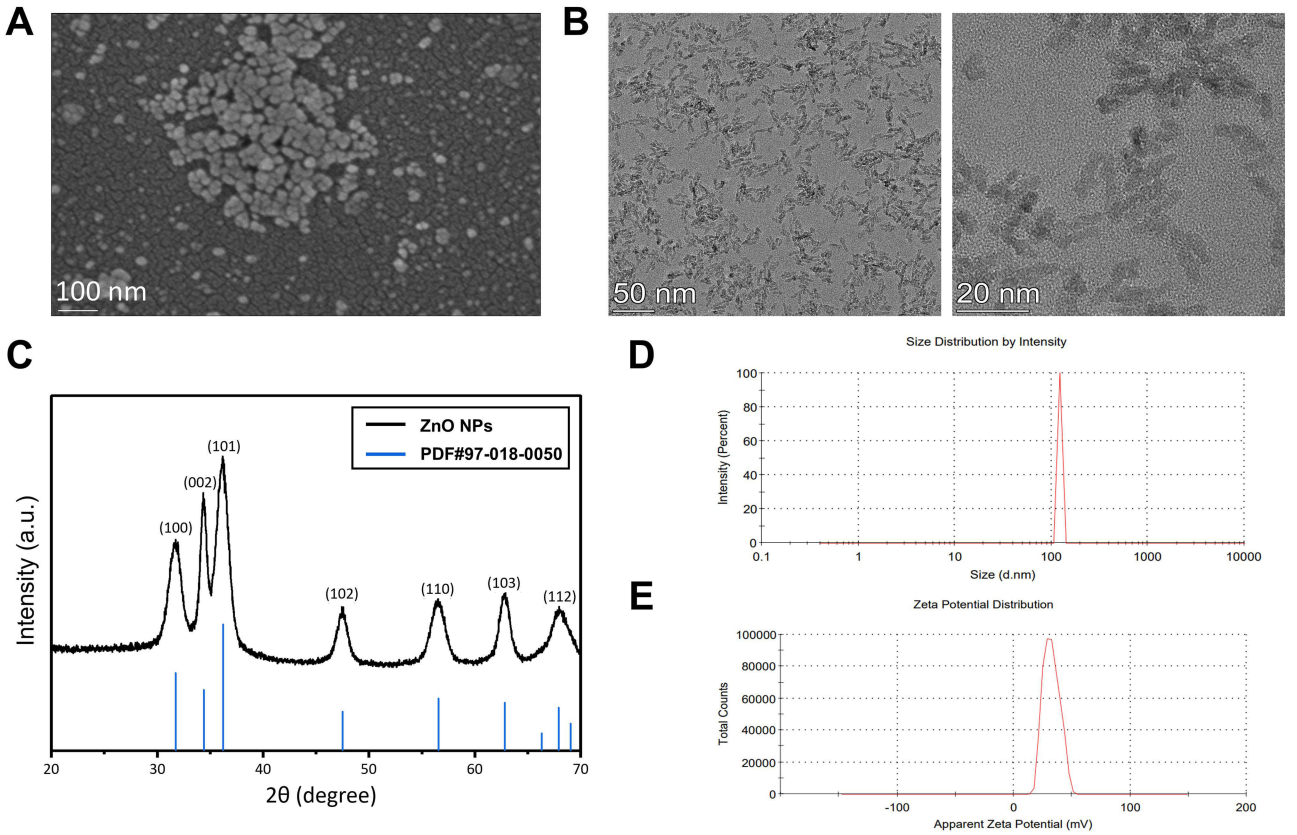

Figure 1 Characterization of ZnO NCs. (**A**) SEM images of prepared ZnO NCs; (**B**) TEM images of prepared ZnO NCs; (**C**) XRD images of the prepared ZnO NCs, which show the characteristic peaks of the prepared ZnO NCs and the standard products; (**D**) Hydrated particle size of ZnO NCs; (**E**) Zeta potential of ZnO NCs.

when dispersed in LB broth, the ZnO NCs showed an increase to 177.7 ± 3.1 nm. Concurrently, the zeta potential reversed to −14.1 ± 0.6 mV. ZnO NCs underwent moderate agglomeration and, decisively, a reversal of surface charge to negative values. This is a classic signature of the formation of a biomolecular corona, where biomolecules from the medium adsorb onto the nanoparticle surface, effectively creating a new biological identity.[39] This state is representative of the physiologically relevant form that interacts with bacterial cells.

Antibacterial and Bactericidal Effects of Synthesized ZnO NCs

The antibacterial and bactericidal activities of the synthesized ZnO NCs were evaluated using *Staphylococcus aureus* (*S. aureus*, Gram-positive) and *E. coli* (Gram-negative) as model bacteria. Following preliminary inhibition zone assays (Figure S1), the minimum inhibitory concentration (MIC) of ZnO NCs against *S. aureus* and *E. coli* was determined using the resazurin colorimetric method, with values ranging from 15.625 to 500 μg/mL. Subsequently, the minimum bactericidal concentration (MBC) was tested across a range of 15.625 to 250 μg/mL. Resazurin, a redox indicator, appears blue in aerobic conditions and turns pink under hypoxia. In aerobic bacterial cultures, oxygen consumption during respiration induces hypoxia, causing resazurin to turn pink. Conversely, if bacterial growth is inhibited, oxygen remains available, and resazurin retains its blue color. Thus, the MIC was defined as the lowest ZnO NCs concentration that maintained resazurin's blue color. Results showed MIC values of 31.25 μg/mL for *S. aureus* and 62.5 μg/mL for *E. coli*, with MBC values of 62.5 μg/mL and 125 μg/mL, respectively (Figure 2A and B).

Based on MIC and MBC results, subsequent biological assays employed ZnO NCs concentrations ranging from 1/4 MIC to 2 × MIC. The *E. coli* biofilm growth curve (Figure S2) indicated that 48-hour biofilms were optimal to assess the inhibitory efficacy of ZnO NCs against biofilm formation and their eradication activity against preformed biofilms.

Viable bacterial counts in the biofilms after ZnO NCs treatment showed that the ZnO NCs significantly reduced the number of viable cells. Treatment with 1/4 MIC (15.625 μg/mL) of ZnO NCs resulted in a significant decrease in viable

https://doi.org/10.2147/IJN.S583878

https://doi.org/10.2147/IJN.S583878

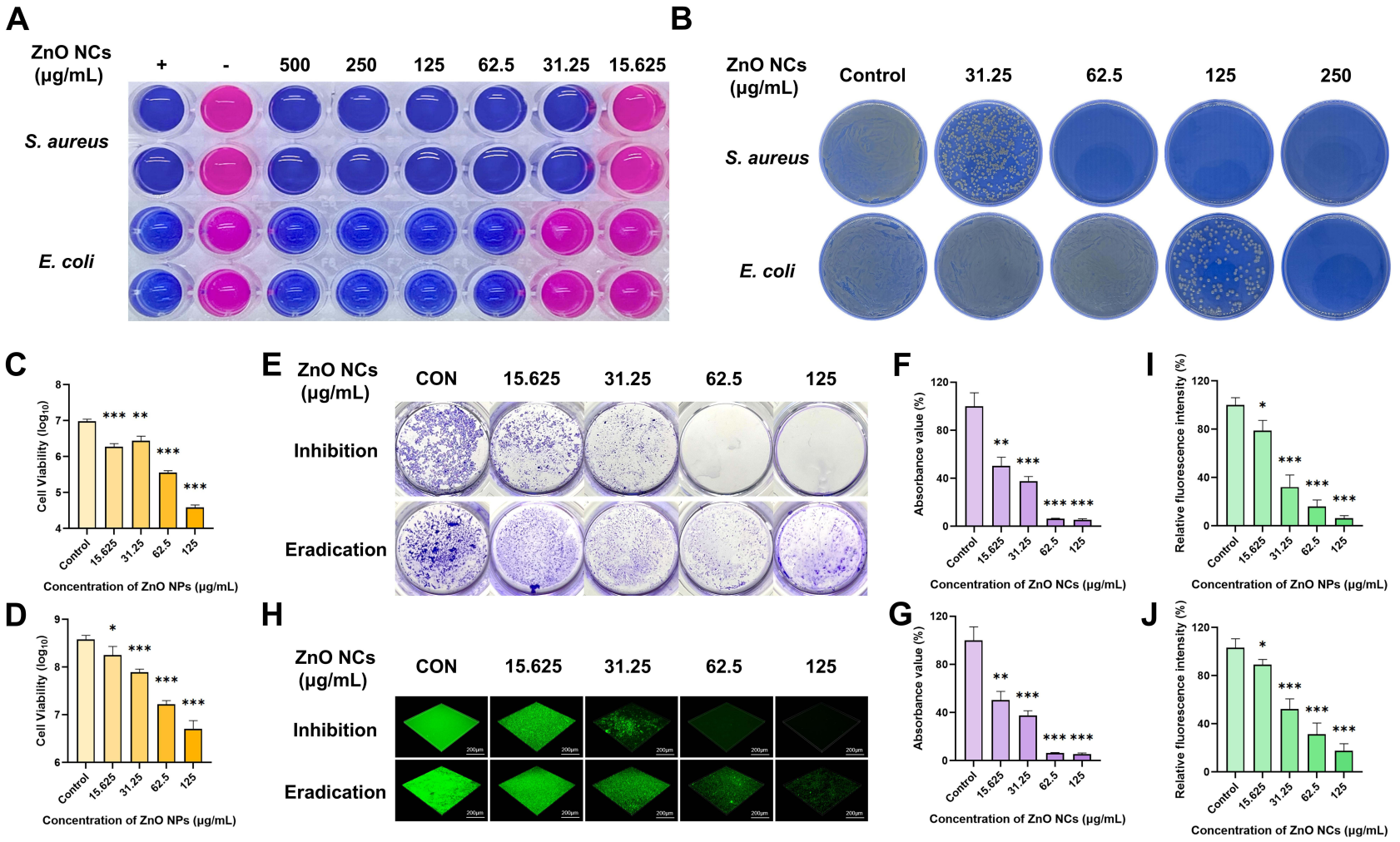

Figure 2 Antibacterial and antibiofilm efficacy of ZnO NCs. (**A**) MIC of ZnO NCs against *S. aureus* and *E. coli*; (**B**) MBC of ZnO NCs against *S. aureus* and *E. coli*; (**C**) Viable bacterial counts after biofilm formation inhibition by ZnO NCs; (**D**) Viable bacterial counts after eradication of mature biofilms by ZnO NCs; (**E**) Crystal violet staining demonstrating the antibiofilm effects of ZnO NCs; (**F**) Relative absorbance at 562 nm of crystal violet staining for inhibited biofilm formation; (**G**) Relative absorbance at 562 nm of crystal violet staining for removed mature biofilms; (**H**) SYTO 9 staining of biofilms treated with ZnO NCs; (**I**) Relative fluorescence intensity of SYTO 9 staining for inhibited biofilm formation; (**J**) Relative fluorescence intensity of SYTO 9 staining for removed mature biofilms. Scale bar = 20 μm. Data are presented as the mean ± SD (n = 3 independent experiments). Statistical significance was determined by one-way ANOVA with Dunnett's post hoc test, with significance levels set at $p < 0.05$ (*), $p < 0.01$ (**), and $p < 0.001$ (***).

counts in both developing and mature biofilms (Figure 2C). At the MBC concentration (125 μg/mL), the viable bacteria in developing biofilms were reduced by more than two orders of magnitude, while those in mature biofilms decreased by nearly two orders of magnitude (Figure 2D).

Crystal violet staining revealed that *E. coli* treated with ZnO NCs at MIC (62.5 μg/mL) and higher concentrations barely formed any biofilm. The biofilm formed after treatment with 1/4 MIC (15.625 μg/mL) ZnO NCs was significantly reduced compared to the control group (Figure 2E and F). Mature biofilms treated with 1/4 MIC (15.625 μg/mL) ZnO NCs showed approximately 40% reduction in total biomass, which was statistically significant. Treatment with ZnO NCs at the MBC concentration (125 μg/mL) removed about 80% of the total biofilm biomass (Figure 2G). Figure S3 shows that residual methanol has no significant effect on the formation of biofilm and the maturation of mature biofilm.

SYTO 9 staining reflected the total bacterial biomass within the biofilms. Upon treatment with a range of ZnO NCs concentrations, the total bacterial biomass in *E. coli* biofilms was significantly reduced (Figure 2H). Treatment with 1/4 MIC (15.625 μg/mL) ZnO NCs led to a 22% reduction in total bacterial biomass in developing biofilms, while 1/2 MIC (31.25 μg/mL) reduced it by approximately 64% (Figure 2I). In mature biofilms, 1/4 MIC (15.625 μg/mL) ZnO NCs reduced the total bacterial biomass by about 10%, which was significantly different from the control. At 1/2 MIC (31.25 μg/mL), more than 50% of the total bacterial biomass was eradicated (Figure 2J). These results demonstrate that sub-MIC concentrations of ZnO NCs exhibit significant efficacy in inhibiting the formation of *E. coli* biofilms and eradicating established biofilms.

ZnO NCs Reduce Biofilm EPS Components

In addition to reducing bacterial counts and total biofilm biomass, ZnO NCs significantly decreased extracellular polymeric substance (EPS) components in both forming and mature *E. coli* biofilms, including proteins, eDNA, and polysaccharides. As shown in Figure 3, sub-MIC concentrations (15.625, 31.25, and 62.5 μg/mL) of ZnO NCs markedly reduced protein, eDNA, and polysaccharide levels in forming biofilms (Figure 3A–C). MIC-level ZnO NCs (62.5 μg/mL) effectively degraded EPS components (proteins, eDNA, polysaccharides) in mature biofilms (Figure 3D–F). These findings collectively indicate that ZnO NCs at sub-MBC concentrations not only inhibit EPS synthesis during biofilm formation but also remove pre-existing EPS in mature biofilms.

The data presented earlier indicate that the inhibition and removal of EPS components by zinc oxide nanocrystals (ZnO NCs) was accompanied by a significant reduction in the number of viable cells within both forming and mature biofilms. A critical mechanistic distinction thus arises: the decrease in EPS could be a passive consequence of the reduced cell density, or it could reflect a direct, active inhibition of the EPS synthesis machinery by ZnO NCs. To explore the latter possibility, we first considered the potential physiological state induced by sub-MIC ZnO NCs.

We hypothesized that sub-MIC ZnO NCs might exert a sub-lethal toxic stress on the bacteria (eg, via Zn^{2+} or localized ROS), which could interfere with intercellular signaling systems like quorum sensing,[40] a global regulator of virulence including EPS production. This disruption could drive bacteria into a metabolically downregulated state that prioritizes survival over virulence, akin to the bioenergetic suppression mediated by endogenous metabolites.[41] Under such stress, bacteria could reprogram their metabolic networks to prioritize survival, potentially downregulating energy-costly virulence functions such as EPS production.[42] Furthermore, the inherent metabolic heterogeneity within biofilms implies that the metabolically active subpopulations at the periphery, which are major contributors to EPS, might be particularly susceptible to this stress.[43] Collectively, these physiological alterations could lead to diminished EPS output. To elucidate the molecular basis underlying these phenotypic changes, we conducted transcriptomic and qPCR analyses, the results of which are presented in a later section.

Confocal laser scanning microscopy (CLSM) images visually demonstrated the changes in the extracellular polymeric substance (EPS) components of *E. coli* biofilms treated with ZnO NCs at the MIC (62.5 μg/mL) (Figure 3G). In the control group, the mature biofilm showed complexed proteins (stained red) and polysaccharides (stained blue) distributed within the dense bacterial cells (stained green), with a biofilm thickness of approximately 30 μm. In addition to inhibiting bacterial growth, treatment with ZnO NCs effectively suppressed the accumulation of protein and polysaccharide components, preventing the development of normal density and thickness. The resulting biofilm appeared thin and loosely structured, with a thickness of only about 10 μm. For pre-formed mature biofilms, ZnO NCs treatment eliminated

https://doi.org/10.2147/IJN.S583878

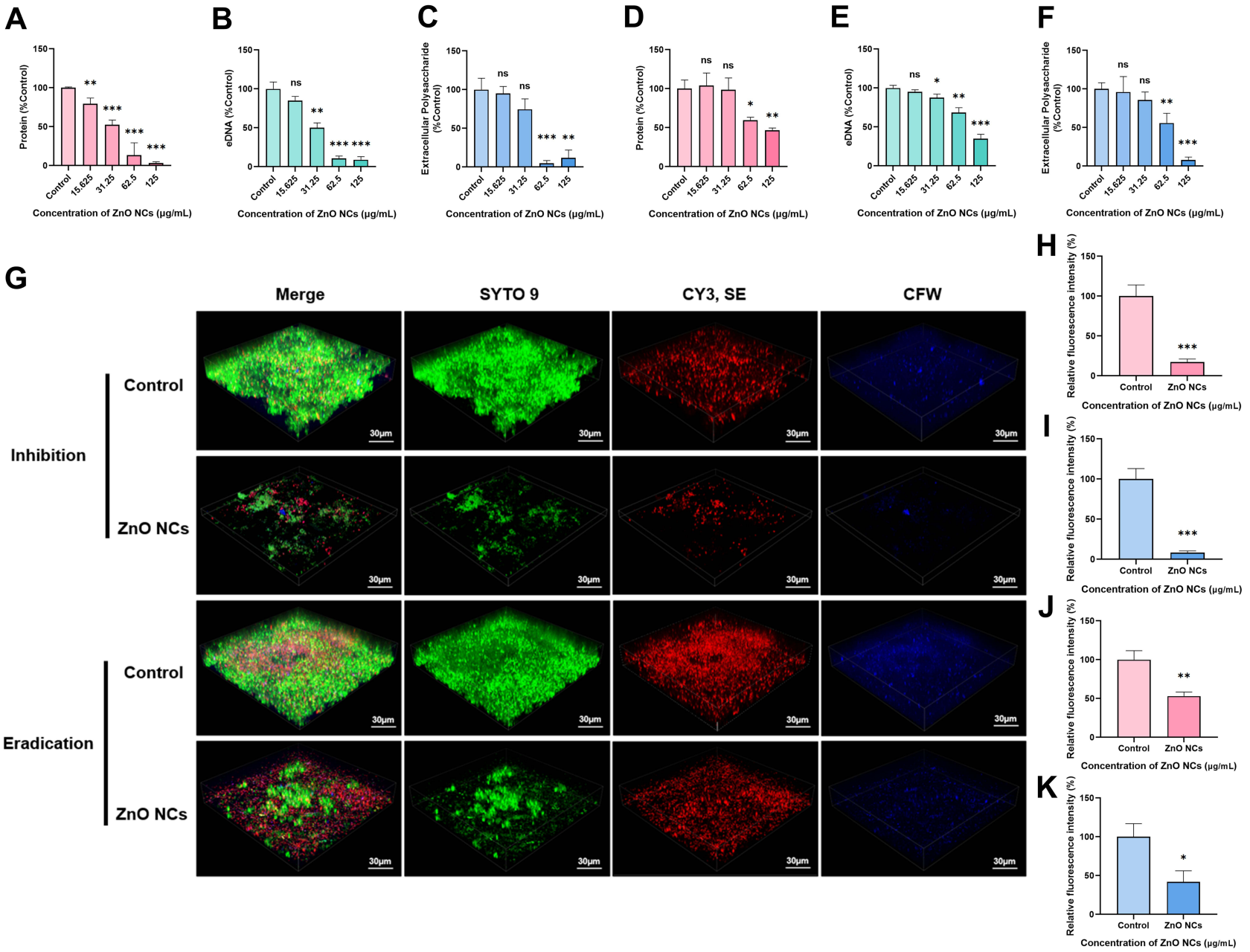

Figure 3 Inhibitory and removal effects of ZnO NCs on EPS in *E. coli* biofilms. (**A**) Relative content of proteins in EPS after inhibition treatment; (**B**) Relative content of eDNA in EPS after inhibition treatment; (**C**) Relative content of extracellular polysaccharides in EPS after inhibition treatment; (**D**) Relative content of proteins in EPS of mature biofilms after removal treatment; (**E**) Relative content of eDNA in EPS of mature biofilms after removal treatment; (**F**) Relative content of extracellular polysaccharides in EPS of mature biofilms after removal treatment; (**G**) Confocal microscopy images of *E. coli* biofilms treated with ZnO NCs, showing bacterial cells (green), proteins (red), and β-polysaccharides (blue). (**H**) Relative fluorescence intensity of proteins in EPS after inhibition treatment; (**I**) Relative fluorescence intensity of β-polysaccharides in EPS after inhibition treatment; (**J**) Relative fluorescence intensity of proteins in EPS of mature biofilms after removal treatment; (**K**) Relative fluorescence intensity of β-polysaccharides in EPS of mature biofilms after removal treatment. Scale bar = 30 μm. Data are presented as the mean ± SD (n = 3 independent experiments). Statistical significance was determined by one-way ANOVA with Dunnett's post hoc test, with significance levels set at $p > 0.05$ (ns), $p < 0.05$ (*), $p < 0.01$ (**), and $p < 0.001$ (***).

most of the bacterial cells and significantly reduced the amount and density of proteins and polysaccharides. The biofilm structure became looser and heterogeneous in thickness, with some localized regions remaining relatively thick due to bacterial aggregation, while other areas were noticeably thinner.

For EPS in the forming biofilm, after treated with ZnO NCs, the relative fluorescence intensity of proteins decreased to 17.296 ± 3.770%, and the relative fluorescence intensity of β-glucan decreased to 8.422 ± 2.016%, both being significantly inhibited, which is consistent with the corresponding changes in relative content (Figure 3H and I). After ZnO NCs treatment for the mature biofilm, the relative fluorescence intensity of proteins decreased to 53.015 ± 5.273%, and the relative fluorescence intensity of β-glucan decreased to 41.765 ± 14.407%, both being significantly inhibited, which is consistent with the corresponding changes in relative content (Figure 3J and K).

Previous studies on ZnO NCs and their composite nanocrystals synthesized by various methods have also reported inhibitory effects on bacterial biofilm EPS to varying degrees,[44–48] which is consistent with the findings of this study. The present study further investigated the spatial distribution of EPS components, providing visual evidence of the suppression and removal of proteins and β-polysaccharides within the EPS, as well as the structural disruption of the biofilm induced by ZnO NCs.

ZnO NCs Inhibit Bacterial Motility of E. coli

The impact of ZnO NCs on the motility of *E. coli* may be related to their ability to disperse biofilms. Therefore, this study evaluated the motility of *E. coli* following treatment with ZnO NCs. Bacterial motility assays included swimming, twitching, and swarming motilities, which reflect flagellar-driven movement, coordinated dense flagellar activity with quorum sensing, and type IV pili-mediated motion, respectively.

As shown in Figure 4A, ZnO NCs inhibited bacterial motility to varying degrees. Specifically, ZnO NCs at 1/2 MIC (31.25 μg/mL) nearly abolished swimming motility (Figure 4B); treatment with 1/4 MIC (15.625 μg/mL) significantly

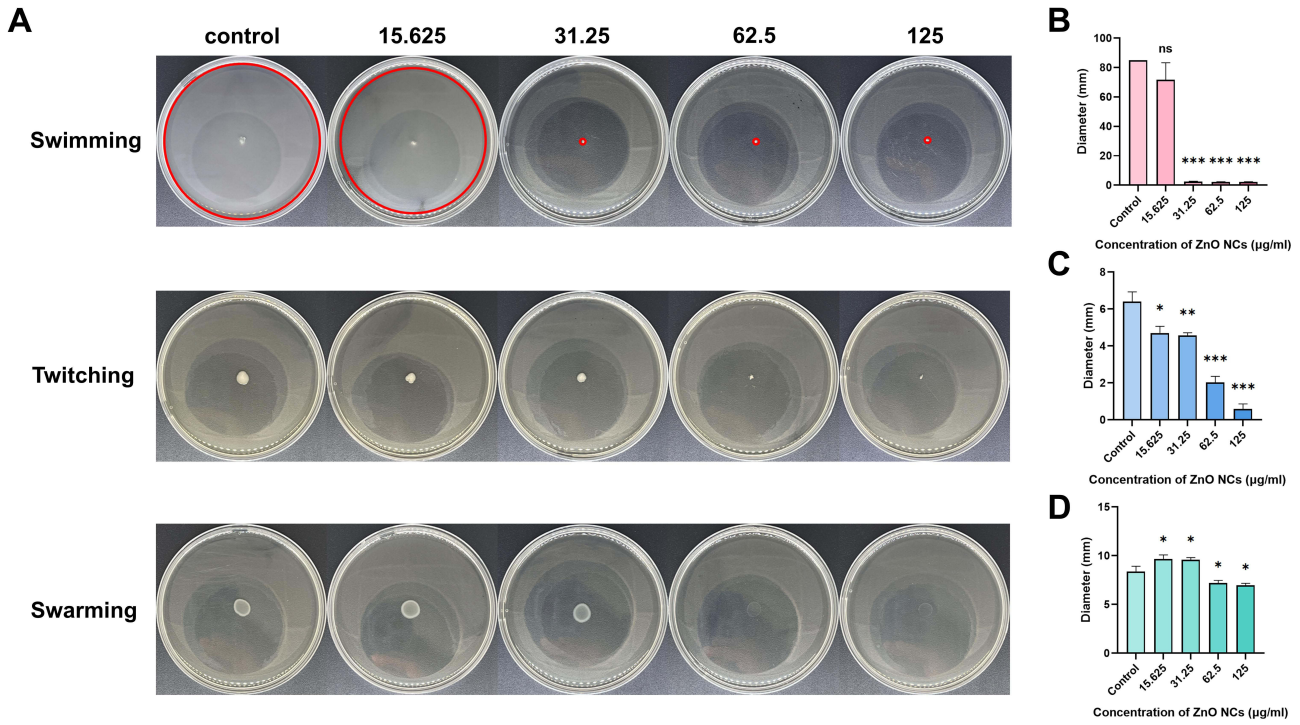

Figure 4 Effects of ZnO NCs on motility of *E. coli*. (**A**) Motility inhibition of *E. coli* (swimming, twitching, and swarming motility) by ZnO NCs; (**B**) Diameter of swimming motility zones; (**C**) Diameter of twitching motility zones; (**D**) Diameter of swarming motility zones. The red circles represent the range of the bacteria's swimming movement. Data are presented as the mean ± SD (n = 3 independent experiments). Statistical significance was determined by one-way ANOVA with Dunnett's post hoc test, with significance levels set at $p > 0.05$ (ns), $p < 0.05$ (*), $p < 0.01$ (**), and $p < 0.001$ (***).

https://doi.org/10.2147/IJN.S583878

reduced twitching motility (Figure 4C); and at the MIC (62.5 μg/mL), swarming motility was also markedly inhibited (Figure 4D). Overall, ZnO NCs at sub-MIC to MIC concentrations significantly suppressed the motility of *E. coli*.

Bacterial motility is closely associated with surface colonization and initial biofilm formation, as well as with the active dispersal and migration of cells from mature biofilms. Inhibition of bacterial motility can prevent bacteria from actively approaching and stably adhering to surfaces.[49] Even if initial attachment occurs, impaired motility disrupts coordinated collective migration and expansion.[50] The loss of twitching ability further hinders cells from rearranging within the biofilm and forming complex three-dimensional structures.[51,52]

The inhibition of swimming, twitching, and swarming motilities by ZnO NCs therefore likely impedes multiple stages of biofilm development, from initial surface colonization to the establishment of mature, complex architectures. In this study, the confirmed suppressive effect of ZnO NCs on *E. coli* motility, as reflected by the significant reduction in motility zone sizes, strongly suggests that the observed reduction in biofilm biomass is consistent with the prevention of robust biofilm formation and structural development. This interpretation aligns with studies on other metal oxide nanoparticles, where motility suppression is recognized as a key contributing mechanism to biofilm inhibition.[53,54]

It is important to note that the smaller motility zones observed likely reflect the integrated impact of ZnO NCs on both bacterial proliferation and motility functions under the conditions of our assay. While our data do not rule out potential direct effects on flagella or pili, the profound inhibition of motility mechanisms supports the conclusion that ZnO NCs act primarily by compromising the biofilm's formative potential and structural integrity, rather than by inducing active dispersal from a mature biofilm.

Mechanism of ZnO NCs Inhibiting E. coli Biofilm

To further investigate the antibiofilm mechanism of ZnO NCs, transcriptomic analysis was performed in this study. Sample correlation analysis between the control group and the ZnO NC-treated group (Figure S4) showed high similarity among the three biological replicates within each group, ensuring the reliability of subsequent differential gene expression analysis. As shown in Figure S5, a total of 2166 differentially expressed genes (DEGs) (FC > 2, FDR < 0.05) were identified in *E. coli* following ZnO NC treatment, among which 1127 were upregulated and 1039 were downregulated.

The KEGG enrichment analysis (Figure 5A) showed significant changes in pathways such as "Biofilm formation – Escherichia coli" and "Flagellar assembly". This suggests that ZnO NC treatment was associated with the downregulation of core genes involved in *E. coli* biofilm formation and key structural components related to bacterial motility. The GO enrichment results (Figure 5B), including terms such as "Locomotion" and "flagellum-dependent cell motility", were consistent with the downregulation of motility-associated genes, aligning with the previously observed phenotype of ZnO NCs inhibiting *E. coli* motility. Additionally, GO analysis indicated a significant downregulation of genes related to amino acid and protein metabolic processes. Moreover, KEGG GSEA (Figure 5C) and GO GSEA (Figure 5D) results suggested that ZnO NC treatment triggered a strong stress response in *E. coli*. While genes related to ribosomal functions, peptide biosynthesis, and ABC transporters were upregulated, potentially reflecting an attempt at cellular repair and survival, key processes such as oxidative phosphorylation, respiratory chain function, and amino acid biosynthesis were significantly suppressed. KEGG enrichment analysis (Figure 5A) revealed significant changes in pathways such as "Biofilm formation – Escherichia coli" and "Flagellar assembly", indicating that ZnO NCs treatment downregulated the expression of core genes involved in *E. coli* biofilm formation and key structural components related to bacterial motility. GO enrichment results (Figure 5B), including terms such as "Locomotion" and all "flagellum-dependent cell motility", further confirmed the downregulation of motility-associated genes, consistent with the previously observed phenotype of ZnO NCs inhibiting *E. coli* motility. Additionally, GO analysis showed significant downregulation of genes related to amino acid and protein metabolic processes in *E. coli* after ZnO NCs treatment. Moreover, KEGG GSEA (Figure 5C) and GO GSEA (Figure 5D) results indicated that ZnO NCs treatment triggered a strong stress response in *E. coli*. Although the bacteria upregulated genes related to ribosomal functions, peptide biosynthesis, and ABC transporters in an attempt to repair and survive, key processes such as oxidative phosphorylation, respiratory chain function, and the supply of essential precursors, particularly amino acid biosynthesis, were significantly suppressed.

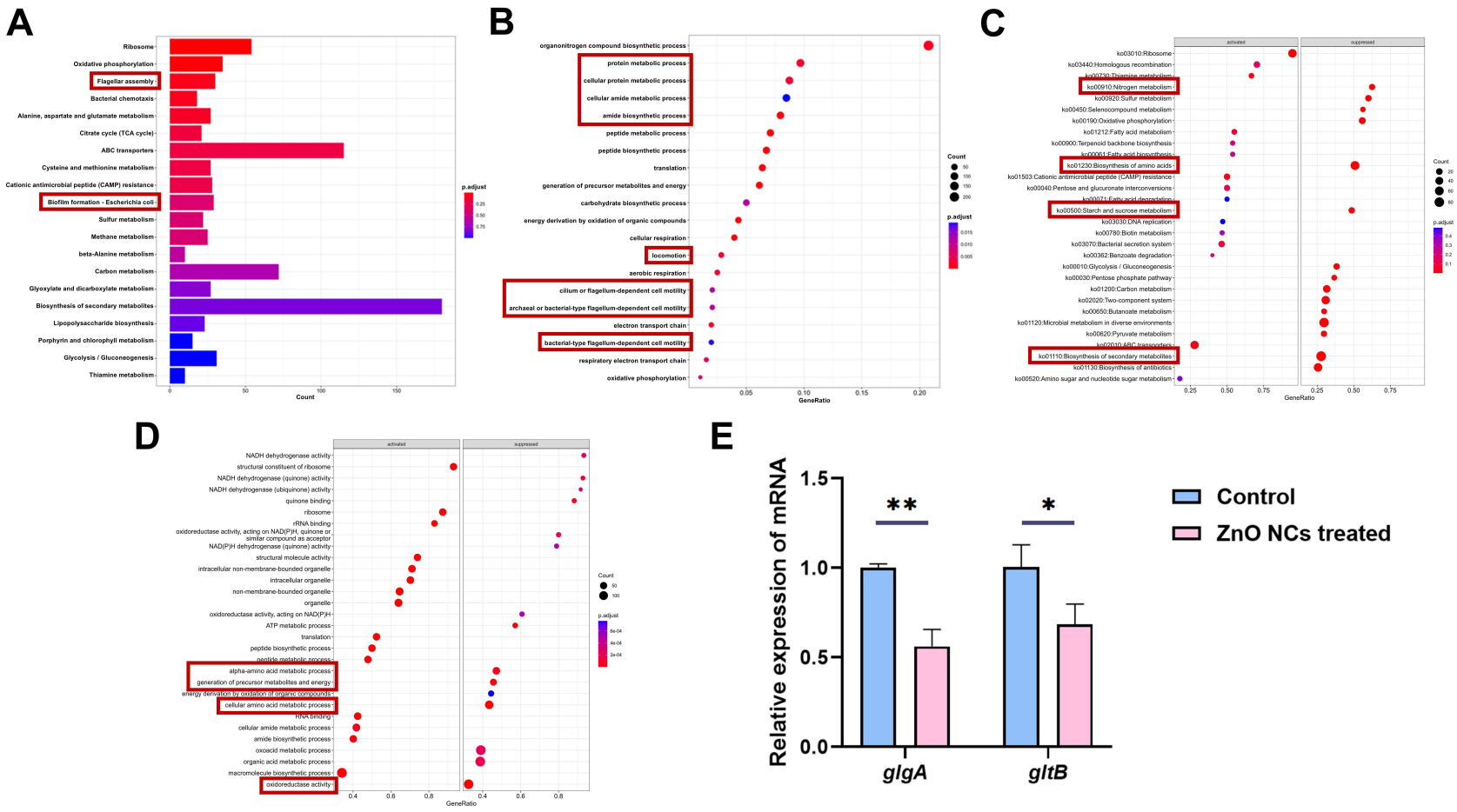

Figure 5 Transcriptomic analysis and qPCR validation of *E. coli* biofilms treated with ZnO NCs. (**A**) KEGG enrichment analysis of transcriptomic data; (**B**) GO enrichment analysis of transcriptomic data; (**C**) KEGG GSEA analysis results; (**D**) GO GSEA analysis results; (**E**) qPCR results of genes related to EPS components in biofilm after ZnO NCs treatment. The red boxes indicate the pathways related to EPS production and bacterial motility. Data are presented as the mean ± SD (n = 3 independent experiments). Statistical significance was determined by one-way ANOVA with Dunnett's post hoc test, with significance levels set at $p < 0.05$ (*), $p < 0.01$ (**).

https://doi.org/10.2147/IJN.S583878

The expression levels of relevant genes were validated using quantitative real-time polymerase chain reaction (qPCR). qPCR results showed significant downregulation of *glgA* and *gltB* gene expression (Figure 5E). The downregulation of *glgA* was associated with multiple significantly enriched functional terms in the transcriptomic analysis, including "Biofilm formation – Escherichia coli" in KEGG, "generation of precursor metabolites and energy", "energy derivation by oxidation of organic compounds", and "carbohydrate biosynthetic process" in GO, as well as "Biosynthesis of secondary metabolites" and "Starch and sucrose metabolism" in KEGG GSEA, and "generation of precursor metabolites and energy" in GO GSEA. Consistent with its known role in glycogen synthesis, the suppression of *glgA* could potentially disrupt carbon storage and availability, which might limit the supply of polysaccharide precursors required for EPS matrix assembly. Similarly, the downregulation of *gltB* was linked to several significantly enriched pathways, including "Alanine, aspartate and glutamate metabolism" in KEGG, "organonitrogen compound biosynthetic process" in GO, "Biosynthesis of amino acids" and "Nitrogen metabolism" in KEGG GSEA, and "oxidoreductase activity", "cellular amino acid metabolic process", and "alpha-amino acid metabolic process" in GO GSEA. Previous studies have shown that deletion of *gltB* inhibits biofilm formation in Bacillus subtilis Bs916 by altering the production of γ-polyglutamic acid and three lipopeptides.[23] Therefore, consistent with its role in glutamate synthase activity, the suppression of *gltB* may disrupt nitrogen assimilation and intracellular amino acid balance, potentially impairing the synthesis of proteinaceous components essential for biofilm integrity.

Together, these findings suggest a model where the downregulation of *glgA* could impair glycogen-dependent carbon provisioning, thereby potentially curtailing the synthesis of polysaccharide components in the EPS. Concurrently, the downregulation of *gltB* may impede glutamate synthase activity, which could disrupt nitrogen assimilation and amino acid metabolism, potentially affecting the production of functional protein elements within the biofilm matrix. Thus, beyond causing broad metabolic dysfunction, ZnO NCs-induced repression of *glgA* and *gltB* may lead to the depletion of both polysaccharide and protein constituents of the EPS. This proposed dual deficiency provides a plausible explanation for how ZnO NCs ultimately inhibit biofilm formation and undermine its structural and functional integrity. It can be inferred that *glgA* downregulation inhibits glycogen-dependent carbon provisioning, thereby curtailing the synthesis of polysaccharide components in the EPS. Meanwhile, *gltB* downregulation impedes glutamate synthase activity, disrupting nitrogen assimilation and amino acid metabolism, which adversely affects the production of functional protein elements within the biofilm matrix. Thus, beyond causing broad metabolic dysfunction, ZnO NCs-induced repression of *glgA* and *gltB* depletes both polysaccharide and protein constituents of the EPS. This dual deficiency ultimately inhibits biofilm formation and undermines the structural and functional integrity of the biofilm.

While our transcriptomic and qPCR data robustly demonstrate the concurrent downregulation of *glgA* and *gltB* genes and the reduction in EPS components upon ZnO NCs treatment, we acknowledge that this evidence establishes a strong correlation rather than definitive causality. The inferred mechanistic link that gene repression directly leads to diminished EPS production is supported by the known functions of these genes in glycogen and glutamate biosynthesis, which are central to extracellular polymeric substance metabolism. To unequivocally prove causality, future studies employing genetic approaches or metabolic rescue experiments would be invaluable. Nevertheless, the consistent and significant correlations observed across our multi-faceted data provide compelling support for the proposed mechanism and offer a clear molecular focus for subsequent in-depth investigation.

Building upon these robust transcriptional correlations, we can now construct a more definitive mechanistic interpretation that bridges our phenotypic observations with the molecular data. These findings bridge the phenotypic observations with molecular mechanisms. Downregulation of *glgA* is predicted to limit glycogen reserves, thereby cutting off the carbon flux necessary for providing key precursors for expolysaccharide synthesis.[55] Downregulation of *gltB* would disrupt nitrogen assimilation and glutamate metabolism, affecting the amino acid supply for matrix protein synthesis.[56] Therefore, at sub-MIC levels, ZnO NCs actively disrupt the biosynthetic capacity for EPS by directly interfering with the expression of core genes such as *glgA* and *gltB*. This direct transcriptional repression provides empirical support for the conjecture of "sub-lethal stress leading to metabolic reprogramming and subsequent EPS inhibition" and pinpoints a core molecular node of action. Although a reduction in viable counts co-occurs, the change in gene expression occurs at the single-cell level, indicating that the direct transcriptional inhibition of EPS synthesis is a separable and primary physiological event from the bactericidal

effect. In summary, we propose that the anti-biofilm efficacy of ZnO NCs stems from a multi-layered interference: the physiological stress they induce directly triggers a transcriptional reprogramming unfavorable for biofilm construction (eg, downregulation of *glgA* and *gltB*), actively dismantling EPS synthesis; concurrently, the accumulated metabolic stress may partly contribute to the decrease in cell viability, which further amplifies the reduction in total biofilm biomass. This approach of sub-lethal virulence suppression aligns with the promising strategy of targeting pathogenicity without exerting strong bactericidal selection pressure, which may help mitigate antibiotic resistance.[57]

Taken together, our integrated transcriptomic and qPCR analyses reveal that ZnO NCs inhibit biofilm formation and disrupt existing biofilms. This effect is strongly associated with the suppression of genes critical for flagellar-dependent motility, glycogen synthesis, and amino acid/protein biosynthesis, pointing to a systemic disruption of the metabolic and structural networks essential for biofilm integrity.

Conclusions

In this study, rod-shaped ZnO NCs were synthesized via a methanol-based solvothermal method. The ZnO NCs showed significant antibacterial activity against both Gram-positive *S. aureus* and Gram-negative *E. coli*, with MIC and MBC values determined. At concentrations ranging from sub-MIC to MBC, the ZnO NCs effectively inhibited the formation of *E. coli* biofilms and disrupted pre-formed mature biofilms, leading to a significant reduction in viable bacterial counts, total biofilm biomass, and overall bacterial load. The antibiofilm effects were strongly associated with a reduction in extracellular polymeric substance (EPS) components, including polysaccharides, proteins, and extracellular DNA (eDNA), which corresponded to decreased EPS density, structural loosening, and increased heterogeneity of the biofilm architecture. Furthermore, ZnO NCs suppressed the motility of *E. coli*, which is believed to restrict biofilm migration and dispersal. Transcriptomic analysis revealed that ZnO NCs downregulated genes associated with biofilm formation, bacterial motility, and amino acid biosynthesis, concurrently with the induction of a stress response that appeared insufficient to restore homeostasis. qPCR validation confirmed significant downregulation of *glgA* and *gltB*. Based on their known functions, the suppression of *glgA* is inferred to limit glycogen-derived carbon flux necessary for extracellular polysaccharide synthesis, and *gltB* downregulation is predicted to disrupt nitrogen assimilation and glutamate-dependent amino acid supply for matrix proteins. Collectively, these transcriptional changes were correlated with impaired EPS integrity and biofilm stability, underscoring the likely contribution of metabolic disruption to ZnO NCs-mediated biofilm inhibition.

This study integrates phenotypic and transcriptomic evidence to reveal key molecular targets and propose a multi-target mechanism, whereby ZnO NCs compromise the biofilm integrity system, including EPS secretion, spatial architecture, and motility, potentially through the associated downregulation of critical genes such as *glgA* and *gltB*. These findings provide a theoretical foundation and valuable insights for the application of ZnO NCs and their composites in combating biofilm-associated contamination and infections.

Data Sharing Statement

The data generated during the present study are available from the corresponding author upon reasonable request.

Acknowledgments

Tianlong Liu and Yeru Wang are the corresponding authors.

We thank Wuhan GeneRead Biotechnology Co., Ltd., for the assistance with RNA-seq assays and data analysis.

Funding

This work was supported by National Key Research and Development Program of China (2024YFF1106705), National Key Research and Development Program of China (2023YFD1301103).

Disclosure

The authors declare no conflicts of interest in this work.

References

1. O'Toole G, Kaplan HB, Kolter R. Biofilm formation as microbial development. *Annu Rev Microbiol*. 2000;54(1):49–79. doi:10.1146/annurev.micro.54.1.49
2. Flemming HC, Wingender J. The biofilm matrix. *Nat Rev Microbiol*. 2010;8(9):623–633. doi:10.1038/nrmicro2415
3. Flemming HC, van Hullebusch ED, Neu TR, et al. The biofilm matrix: multitasking in a shared space. *Nat Rev Microbiol*. 2023;21(2):70–86. doi:10.1038/s41579-022-00791-0
4. Flemming HC, Wingender J, Szewzyk U, Steinberg P, Rice SA, Kjelleberg S. Biofilms: an emergent form of bacterial life. *Nat Rev Microbiol*. 2016;14(9):563–575. doi:10.1038/nrmicro.2016.94
5. Donohue MJ, Pham M, Brown S, Easwaran KM, Vesper S, Mistry JH. Water quality influences Legionella pneumophila determination. *Water Res*. 2023;238:119989. doi:10.1016/j.watres.2023.119989
6. Hall-Stoodley L, Costerton JW, Stoodley P. Bacterial biofilms: from the natural environment to infectious diseases. *Nat Rev Microbiol*. 2004;2(2):95–108. doi:10.1038/nrmicro821
7. Römling U, Balsalobre C. Biofilm infections, their resilience to therapy and innovative treatment strategies. *J Intern Med*. 2012;272(6):541–561. doi:10.1111/joim.12004
8. Hentzer M, Teitzel GM, Balzer GJ, et al. Alginate overproduction affects pseudomonas aeruginosa biofilm structure and function. *J Bacteriol*. 2001;183(18):5395–5401. doi:10.1128/jb.183.18.5395-5401.2001
9. Hinsa SM, Espinosa-Urgel M, Ramos JL, O'Toole GA. Transition from reversible to irreversible attachment during biofilm formation by *Pseudomonas fluorescens* WCS365 requires an ABC transporter and a large secreted protein. *Mol Microbiol*. 2003;49(4):905–918. doi:10.1046/j.1365-2958.2003.03615.x
10. Barnhart MM, Chapman MR. Curli biogenesis and function. *Annu Rev Microbiol*. 2006;60(1):131–147. doi:10.1146/annurev.micro.60.080805.142106
11. Nhu NTK, Phan MD, Peters KM, et al. Discovery of new genes involved in curli production by a uropathogenic Escherichia coli strain from the highly virulent O45:K1:H7 lineage. *mBio*. 2018;9(4):e01462–18. doi:10.1128/mBio.01462-18
12. Whitchurch CB, Tolker-Nielsen T, Ragas PC, Mattick JS. Extracellular DNA required for bacterial biofilm formation. *Science*. 2002;295(5559):1487. doi:10.1126/science.295.5559.1487
13. Ciofu O, Moser C, Jensen PØ, Høiby N. Tolerance and resistance of microbial biofilms. *Nat Rev Microbiol*. 2022;20(10):621–635. doi:10.1038/s41579-022-00682-4
14. Persat A, Nadell CD, Kim MK, et al. The mechanical world of bacteria. *Cell*. 2015;161(5):988–997. doi:10.1016/j.cell.2015.05.005
15. Guttenplan SB, Kearns DB. Regulation of flagellar motility during biofilm formation. *FEMS Microbiol Rev*. 2013;37(6):849–871. doi:10.1111/1574-6976.12018
16. Ha DG, O'Toole GA. c-di-GMP and its effects on biofilm formation and dispersion: a pseudomonas aeruginosa review. *Microbial Biofilms*. 2015:301–317. doi:10.1128/microbiolspec.mb-0003-2014
17. Mah TFC, O'Toole GA. Mechanisms of biofilm resistance to antimicrobial agents. *Trends Microbiol*. 2001;9(1):34–39. doi:10.1016/S0966-842X(00)01913-2
18. Sharma S, Mohler J, Mahajan SD, Schwartz SA, Bruggemann L, Aalinkeel R. Microbial biofilm: a review on formation, infection, antibiotic resistance, control measures, and innovative treatment. *Microorganisms*. 2023;11(6):1614. doi:10.3390/microorganisms11061614
19. Sutherland I. The biofilm matrix – an immobilized but dynamic microbial environment. *Trends Microbiol*. 2001;9(5):222–227. doi:10.1016/S0966-842X(01)02012-1
20. Berk V, Fong JCN, Dempsey GT, et al. Molecular architecture and assembly principles of vibrio cholerae biofilms. *Science*. 2012;337(6091):236–239. doi:10.1126/science.1222981
21. Wyman M, Thom C. Temporal orchestration of glycogen synthase (GlgA) gene expression and glycogen accumulation in the oceanic picoplanktonic Cyanobacterium Synechococcus sp. Strain WH8103. *Appl Environ Microbiol*. 2012;78(13):4744–4747. doi:10.1128/AEM.00254-12
22. Huang Y, Suo Y, Shi C, Szlavik J, Shi XM, Knøchel S. Mutations in gltB and gltC reduce oxidative stress tolerance and biofilm formation in *Listeria monocytogenes* 4b G. *Int J Food Microbiol*. 2013;163(2):223–230. doi:10.1016/j.ijfoodmicro.2013.02.023
23. Zhou H, Luo C, Fang X, et al. Loss of GltB inhibits biofilm formation and biocontrol efficiency of bacillus subtilis Bs916 by altering the production of γ-polyglutamate and three lipopeptides. *PLoS One*. 2016;11(5):e0156247. doi:10.1371/journal.pone.0156247
24. Wen X, Tang T, Bao T, et al. gltB encoding glutamate synthase is involved in persister and biofilm formation and virulence in Staphylococcus aureus. *Microbiol Spectr*. 2025;13(9):e00511–25. doi:10.1128/spectrum.00511-25
25. Xiang Y, Pan Z, Qi X, et al. A cuttlefish ink nanoparticle-reinforced biopolymer hydrogel with robust adhesive and immunomodulatory features for treating oral ulcers in diabetes. *Bioact Mater*. 2024;39:562–581. doi:10.1016/j.bioactmat.2024.04.022
26. Cheng S, Wang H, Pan X, et al. Dendritic hydrogels with robust inherent antibacterial properties for promoting bacteria-infected wound healing. *ACS Appl Mater Interfaces*. 2022;14(9):11144–11155. doi:10.1021/acsami.1c25014
27. Singh THA, Das J, Sil PC. Zinc oxide nanoparticles: a comprehensive review on its synthesis, anticancer and drug delivery applications as well as health risks. *Adv Colloid Interface Sci*. 2020;286:102317. doi:10.1016/j.cis.2020.102317
28. Husain FM, Qais FA, Ahmad I, et al. Biosynthesized zinc oxide nanoparticles disrupt established biofilms of pathogenic bacteria. *Appl Sci*. 2022;12(2):710. doi:10.3390/app12020710
29. Nath R, Lahiri D, Nag M, et al. Antibiofilm activity of exopolysaccharide-mediated ZnO nanoparticle against Pseudomonas aeruginosa biofilm. *Naunyn Schmiedebergs Arch Pharmacol*. 2024. doi:10.1007/s00210-024-03651-1
30. Lu X, Weakley AT, Aston DE, Rasco BA, Wang S, Konkel ME. Examination of nanoparticle inactivation of Campylobacter jejuni biofilms using infrared and Raman spectroscopies. *J Appl Microbiol*. 2012;113(4):952–963. doi:10.1111/j.1365-2672.2012.05373.x
31. Husain FM, Hasan I, Qais FA, Khan RA, Alam P, Alsalme A. Fabrication of zinc oxide-xanthan gum nanocomposite via green route: attenuation of quorum sensing regulated virulence functions and mitigation of biofilm in gram-negative bacterial pathogens. *Coatings*. 2020;10(12):1190. doi:10.3390/coatings10121190
32. Sirelkhatim A, Mahmud S, Seeni A, et al. Review on zinc oxide nanoparticles: antibacterial activity and toxicity mechanism. *Nano-Micro Lett*. 2015;7(3):219–242. doi:10.1007/s40820-015-0040-x

33. Afrasiabi S, Partoazar A. Targeting bacterial biofilm-related genes with nanoparticle-based strategies. *Front Microbiol*. 2024;15:1387114. doi:10.3389/fmicb.2024.1387114
34. Abd El-Hamid MI, Y. El-Naenaeey ES, M Kandeel T, et al. Promising antibiofilm agents: recent breakthrough against biofilm producing methicillin-resistant Staphylococcus aureus. *Antibiotics*. 2020;9(10):667. doi:10.3390/antibiotics9100667
35. Badawy MSEM, Riad OKM, Taher FA, Zaki SA. Chitosan and chitosan-zinc oxide nanocomposite inhibit expression of LasI and RhlI genes and quorum sensing dependent virulence factors of Pseudomonas aeruginosa. *Int J Biol Macromol*. 2020;149:1109–1117. doi:10.1016/j.ijbiomac.2020.02.019
36. Bai X, Li L, Liu H, Tan L, Liu T, Meng X. Solvothermal synthesis of ZnO nanoparticles and anti-infection application in vivo. *ACS Appl Mater Interfaces*. 2015;7(2):1308–1317. doi:10.1021/am507532p
37. Wang J, Li G, Yin H, An T. Bacterial response mechanism during biofilm growth on different metal material substrates: EPS characteristics, oxidative stress and molecular regulatory network analysis. *Environ Res*. 2020;185:109451. doi:10.1016/j.envres.2020.109451
38. Saeki EK, Yamada AY, de Araujo LA, et al. Subinhibitory concentrations of biogenic silver nanoparticles affect motility and biofilm formation in Pseudomonas aeruginosa. *Front Cell Infect Microbiol*. 2021;11:656984. doi:10.3389/fcimb.2021.656984
39. Kopac T. Protein Corona, understanding the nanoparticle–protein interactions and future perspectives: a critical review. *Int J Biol Macromol*. 2021;169:290–301. doi:10.1016/j.ijbiomac.2020.12.108
40. Abisado RG, Benomar S, Klaus JR, Dandekar AA, Chandler JR. Bacterial quorum sensing and microbial community interactions. *mBio*. 2018;9(3):e02331–17. doi:10.1128/mBio.02331-17
41. Horak RD, Ciemniecki JA, Newman DK. Bioenergetic suppression by redox-active metabolites promotes antibiotic tolerance in Pseudomonas aeruginosa. *Proc Natl Acad Sci U S A*. 2024;121(46):e2406555121. doi:10.1073/pnas.2406555121
42. Rihacek M, Kosaristanova L, Fialova T, et al. Metabolic adaptations of Escherichia coli to extended zinc exposure: insights into tricarboxylic acid cycle and trehalose synthesis. *BMC Microbiol*. 2024;24(1):384. doi:10.1186/s12866-024-03463-6
43. Evans C, Kempes C, Price-Whelan A, Dietrich L. Metabolic heterogeneity and cross-feeding in bacterial multicellular systems. *Trends Microbiol*. 2020;28(9):732–743. doi:10.1016/j.tim.2020.03.008
44. Tabrez Khan S, Ahamed M, Al-Khedhairy A, Musarrat J. Biocidal effect of copper and zinc oxide nanoparticles on human oral microbiome and biofilm formation. *Mater Lett*. 2013;97:67–70. doi:10.1016/j.matlet.2013.01.085
45. Hayat S, Ashraf A, Zubair M, et al. Biofabrication of ZnO nanoparticles using Acacia arabica leaf extract and their antibiofilm and antioxidant potential against foodborne pathogens. *PLoS One*. 2022;17(1):e0259190. doi:10.1371/journal.pone.0259190
46. Chegini V, Noghabi KA, Afshari KP, Ebadi M, Noghabi KA. Biological synthesis of ZnO nanoparticles using ethanolic extract of *Satureja sahendica* Bornm: its characterization and antimicrobial features. *Biomass Convers Bioref*. 2023;13(17):16037–16048. doi:10.1007/s13399-021-02187-1
47. Maghrawy HH, El Kareem HA, Gomaa OM. Enhanced exopolysaccharide production in gamma irradiated Bacillus subtilis: a biofilm-mediated strategy for ZnO nanoparticles removal. *Int J Biol Macromol*. 2024;258:128884. doi:10.1016/j.ijbiomac.2023.128884
48. Lahiri D, Ray RR, Sarkar T, et al. Anti-biofilm efficacy of green-synthesized ZnO nanoparticles on oral biofilm: in vitro and in silico study. *Front Microbiol*. 2022;13. doi:10.3389/fmicb.2022.939390
49. O'Toole GA, Kolter R. Flagellar and twitching motility are necessary for Pseudomonas aeruginosa biofilm development. *Mol Microbiol*. 1998;30(2):295–304. doi:10.1046/j.1365-2958.1998.01062.x
50. Harshey RM. Bacterial motility on a surface: many ways to a common goal. *Annu Rev Microbiol*. 2003;57(1):249–273. doi:10.1146/annurev.micro.57.030502.091014
51. Rossy T, Distler T, Meirelles LA, et al. Pseudomonas aeruginosa type IV pili actively induce mucus contraction to form biofilms in tissue-engineered human airways. *PLOS Biol*. 2023;21(8):e3002209. doi:10.1371/journal.pbio.3002209
52. Anyan ME, Amiri A, Harvey CW, et al. Type IV pili interactions promote intercellular association and moderate swarming of Pseudomonas aeruginosa. *Proc Natl Acad Sci U S A*. 2014;111(50):18013–18018. doi:10.1073/pnas.1414661111
53. Falcón García C, Kretschmer M, Lozano-Andrade CN, et al. Metal ions weaken the hydrophobicity and antibiotic resistance of Bacillus subtilis NCIB 3610 biofilms. *NPJ Biofilms Microbiomes*. 2020;6(1):1. doi:10.1038/s41522-019-0111-8
54. Rasko DA, Sperandio V. Anti-virulence strategies to combat bacteria-mediated disease. *Nat Rev Drug Discov*. 2010;9(2):117–128. doi:10.1038/nrd3013
55. Xu Y, Tiago Guerra L, Li Z, Ludwig M, Charles Dismukes G, Bryant DA. Altered carbohydrate metabolism in glycogen synthase mutants of Synechococcus sp. strain PCC 7002: cell factories for soluble sugars. *Metab Eng*. 2013;16:56–67. doi:10.1016/j.ymben.2012.12.002
56. Reitzer L. Nitrogen assimilation and global regulation in Escherichia coli. *Annu Rev Microbiol*. 2003;57(1):155–176. doi:10.1146/annurev.micro.57.030502.090820
57. Clatworthy AE, Pierson E, Hung DT. Targeting virulence: a new paradigm for antimicrobial therapy. *Nat Chem Biol*. 2007;3(9):541–548. doi:10.1038/nchembio.2007.24